

Generation of different Bell states within the SPDC phase-matching bandwidth

G. Brida, M. Genovese and L. A. Krivitsky

Istituto Nazionale di Ricerca Metrologica, Strada delle Cacce 91, 10135 Torino, Italy

M. V. Chekhova

Department of Physics,

M.V.Lomonosov Moscow State University,

Leninskie Gory, 119992 Moscow, Russia

We study the frequency-angular lineshape for a phase-matched nonlinear process producing entangled states and show that there is a continuous variety of maximally-entangled states generated for different mismatch values within the natural bandwidth. Detailed considerations are made for two specific methods of polarization entanglement preparation, based on type-II spontaneous parametric down-conversion (SPDC) and on SPDC in two subsequent type-I crystals producing orthogonally polarized photon pairs. It turns out that different Bell states are produced at the center of the SPDC line and on its slopes, corresponding to about half-maximum intensity level. These Bell states can be filtered out by either frequency selection or angular selection, or both. Our theoretical calculations are confirmed by a series of experiments, performed for the two above-mentioned schemes of producing polarization-entangled photon pairs and with two kinds of measurements: frequency-selective and angular-selective.

PACS numbers: 42.50.Dv, 03.67.Hk, 42.62.Eh

I. INTRODUCTION

Spontaneous Parametric Down-Conversion (SPDC) provides the easiest way of generating polarization-entangled two-photon states, which are a fundamental resource for quantum communication or quantum computation [1], studies on foundations of quantum mechanics [2], quantum metrology [3], quantum imaging [4], etc.

Various experimental schemes can be used for this purpose [2]. The first efficient scheme suggested was the one based on non-collinear type-II SPDC [6]. In this scheme, entangled two-photon states were generated in two angular (wavevector) modes and two polarization modes (polarization-wavevector entanglement). Later, 'interferometric' schemes were also proposed, where two crystals were involved or two passages of the pump beam through the same crystal. In most of these schemes, the set of modes for entanglement also included two polarization modes and two wavevector modes. Among numerous configurations, one should mention schemes with type-II crystals specially designed for the operation in the femtosecond-pulsed regime [7, 8] and the scheme with two type-I crystals [9]. Less common but very useful for certain applications are interferometric schemes that provide entanglement in a set of two frequency modes and two polarization modes (polarization-frequency entanglement) [10, 11].

We would like to emphasize that in all such experiments the goal was to achieve a certain Bell state generated within the whole bandwidth given by phase matching. By changing the settings of the optical elements, other Bell states can be obtained, but still for the whole phase-matched range of wavelengths and wavevectors. In

type-II-based schemes, this is provided by inserting a birefringent optical element compensating for the delay between orthogonally polarized photons of an entangled pair ('e-o delay compensation') [12]. Otherwise, entanglement is obtained only for the narrow frequency domain around exact degeneracy, selected by means of narrow-band filters. In type-I schemes, e-o delay compensation or filtering are seemingly not necessary but, as we will show further, still preferable since entanglement is not uniform over the whole bandwidth and changes on the slopes of the SPDC phase-matching line.

In this paper, we are interested in the fine structure of the phase-matching line from the viewpoint of various Bell states generation. We find that without the e-o delay compensation, an interesting effect occurs within the bandwidth for every phase-matched nonlinear process: the same phase mismatch that is responsible for the intensity decrease induces a phase shift between the components of the produced entangled state. In particular, we will discuss in detail the SPDC case. In this case, we show that various maximally-entangled states and, in particular, two different Bell states are generated within the spectrum allowed by phase-matching and that one can choose them by means of frequency or angular selection. This occurs for all schemes of polarization-entangled states generation - based on type-II phase matching and based on the 'two type-I crystals' configuration - and involves both frequency or angular lineshapes of SPDC. For example, both for type II and 'two-type I' near-collinear production one finds inside the natural bandwidth maximally entangled states ($\frac{|HV\rangle + e^{i\phi}|VH\rangle}{\sqrt{2}}$ and $\frac{|HH\rangle + e^{i\phi}|VV\rangle}{\sqrt{2}}$ respectively), whose relative phase between components, ϕ , ranges from 0 to π .

After a detailed theoretical discussion, we present experimental data demonstrating it in various cases.

The paper is organized as follows. In Section II, we present the theory of the effect and describe a general scheme for its observation. In particular, the two-dimensional (frequency-angular) spectrum of SPDC is presented, with the calculated domains of various Bell states generation shown. Sections III and IV are devoted to the experimental observation of the effect. Section III is focused on the frequency spectrum of collinear SPDC, both for type-II and 'two type-I' schemes. The effect is observed in two ways: by scanning the frequency of one of the entangled photons and by scanning the arrival-time difference of the pair, after transmitting it through an optical fibre. Section IV contains experimental results on the SPDC angular spectrum. In this group of measurements, also carried out both for type-II phase matching and the 'two type-I configuration', switching between different Bell states is performed by scanning the wavevector direction of one of the two photons. Finally, in Section V we draw the conclusions and discuss possible applications of the observed effect.

II. THEORY

Let us consider polarization-entangled two-photon state generated via a phase-matched process, which can be, for instance, SPDC or four-wave mixing [13]. Ignoring the vacuum component, we can write the state in the general form (see, e.g., [14]),

$$|\Psi\rangle = \int d\mathbf{k}d\mathbf{k}' \int d\mathbf{r} F_{NL}(\mathbf{r}) e^{i\mathbf{\Delta}(\mathbf{k},\mathbf{k}')\mathbf{r}} a_{P,\mathbf{k}}^\dagger a_{P',\mathbf{k}'}^\dagger |\text{vac}\rangle, \quad (1)$$

(with polarizations $P = H, P' = V$ for type II and $P = P'$ for type I phase matching, respectively), where $\mathbf{\Delta}(\mathbf{k}, \mathbf{k}')$ is the phase mismatch depending on wavevector and frequency modes \mathbf{k}, \mathbf{k}' , in which a pair is created, $a_{P,\mathbf{k}}^\dagger$ are photon creation operators and $F_{NL}(\mathbf{r})$ is the factor containing nonlinearity and the pump (pumps) field distribution over the nonlinear medium. Integration over the volume turns $F_{NL}(\mathbf{r})$ into its Fourier transform, $F_{NL}(\mathbf{k}, \mathbf{k}')$, but there remains a phase factor, depending on \mathbf{k}, \mathbf{k}' . If this phase factor is not symmetric w.r.t. the exchange $\mathbf{k} \leftrightarrow \mathbf{k}'$, as it indeed happens in nearly all cases, then the phase between the two components of an entangled state generated at the output will change within the phase-matched bandwidth.

Let us now consider the case where polarization-entangled states are generated through SPDC. We will separately focus on the situations of type-II phase matching (in a single crystal) and of type-I phase matching (in two crystals pumped by the same pump and the optic axes oriented in orthogonal planes).

II.1 Type II phase matching

Consider first polarization-entangled photons produced via type-II SPDC in a homogeneous crystal of length L from a cw pump with relatively large beam diameter $a \gg L \tan \theta$, θ being the typical angle of scattering, so that exact transverse phase matching can be assumed [15]. Integration over the volume leads to a delta-function of the transverse mismatch, $\delta^{(2)}(\mathbf{k}_\perp + \mathbf{k}'_\perp)$, and due to the strict frequency correlation between the two photons, integration over the modes \mathbf{k}' in Eq.(1) disappears. In the two-photon amplitude, only the longitudinal part of the wavevector mismatch is relevant, $\Delta_z(\mathbf{k})$, where z is the direction along the pump wavevector. In terms of experimentally measurable quantities, integration in \mathbf{k} means integration w.r.t. the angle of scattering and frequency of one of the photons belonging to the entangled pair. Further, assuming that the signal and idler photons have wavevectors belonging to the plain of the optic axis and labeling them as o and e (ordinary and extraordinary), we can write the state as

$$|\Psi\rangle = \iint d\theta d\Omega e^{i\frac{\Delta_z L}{2}} \text{sinc}\left(\frac{\Delta_z L}{2}\right) \times a_e^\dagger(\theta, \omega_0 + \Omega) a_o^\dagger(-\theta, \omega_0 - \Omega) |\text{vac}\rangle, \quad (2)$$

where ω_0 is the central frequency of SPDC spectrum, the sinc function is defined as $\text{sinc}(x) \equiv \frac{\sin x}{x}$, and the longitudinal phase mismatch has the form

$$\Delta_z \equiv \Delta_z(\theta, \Omega) = k_e(\theta, \omega_0 + \Omega) \cos \theta + k_o(-\theta, \omega_0 - \Omega) \cos \theta - k_p, \quad (3)$$

k_p, k_e , and k_o being the wavevectors of the pump, signal (extraordinary), and idler (ordinary) photons, respectively. From this, one can see that with the change in the mismatch Δ_z , determining the lineshape of SPDC, there occurs a simultaneous change in the phase factor standing by the state. If we take into account both positive and negative values of the mismatch, we find that different types of two-photon states can be generated within the spectrum allowed by phase-matching. For instance, the state generated at exact phase matching ($\Delta_z = 0$) is a factorable one, but it can be turned into the Bell state $|\Psi^+\rangle$ by means of a beamsplitter. At mismatch values $\Delta_z = \pm\pi/L$, which can be realized by means of frequency offset from degeneracy, or angular offset, or both, the state already becomes another Bell one, the singlet state $|\Psi^-\rangle$. At intermediate mismatch values, various maximally entangled states $\frac{|HV\rangle + e^{i\phi}|VH\rangle}{\sqrt{2}}$ are generated, their phases ϕ being between 0 and π .

Expanding the mismatch (3) around the collinear frequency-degenerate point, where exact phase matching is assumed, up to linear terms in frequency and angular offsets, we obtain

$$\Delta_z(\theta, \Omega) \simeq D\Omega + B\theta, \quad (4)$$

where $D \equiv \frac{dk_e}{d\Omega} - \frac{dk_o}{d\Omega}$, $B \equiv \frac{dk_e}{d\theta}$.

One can observe that the singlet state $|\Psi^-\rangle$ is generated for a continuous set of frequencies and angles θ, Ω , for which $\Delta_z(\theta, \Omega) = \pm\pi/L$. This is shown in Fig.1a where the frequency-angular spectrum of SPDC is calculated for the case of collinear frequency-degenerate type-II phase matching in a 0.5 mm BBO crystal. The solid line corresponds to $\Delta_z(\theta, \Omega) = 0$, i.e. $|\Psi^+\rangle$ production; dashed lines correspond to $\Delta_z(\theta, \Omega) = \pm\pi/L$, i.e. $|\Psi^-\rangle$ generation. Note that at angles and frequencies corresponding to $|\Psi^-\rangle$ generation, the intensity of SPDC is only about 0.4 times as large as the intensity at the maximum.

Frequency spectra. For the sake of simplicity let us start by considering the collinear case, i.e. the angle between the photons $\theta = 0$. In experiment, this can be provided by a pinhole inserted into the SPDC beam. In this case the two-photon state (2) can be written as a frequency expansion:

$$|\Psi\rangle = \int_0^\infty d\Omega \text{sinc}(\tau_0\Omega) [a_H^\dagger(\omega_0 + \Omega)a_V^\dagger(\omega_0 - \Omega)e^{i\tau_0\Omega} + a_V^\dagger(\omega_0 + \Omega)a_H^\dagger(\omega_0 - \Omega)e^{-i\tau_0\Omega}] |\text{vac}\rangle, \quad (5)$$

where $\tau_0 \equiv DL/2$ is the e-o delay for a pair born at the center of the crystal. Here, we assume the e-photon to be horizontally polarized; the integration runs only on positive frequency offsets.

We see that while at the degenerate frequency, the state $|\Psi^+\rangle$ is created (if the photon flux is split in two beams by a beamsplitter), the state generated at $\Omega = \pm\pi/2\tau_0$, i.e., at approximately half-maximum of the intensity, is the singlet state $|\Psi^-\rangle$.

If a birefringent plate is inserted into the beam after the crystal, then an additional e-o delay τ will be added to τ_0 in Eq. (2). The case $\tau = -\tau_0$ is well known: it means that the e-o delay arising in the crystal is completely compensated. Then, for the whole bandwidth allowed by phase matching, one produces a $|\Psi^+\rangle$. More interesting for our considerations is the case where τ has the same sign as τ_0 . In this case the change of the relative phase between the two state components in Eq.(2) becomes more rapid than the intensity variation determined by the phase matching, and both $|\Psi^+\rangle$ and $|\Psi^-\rangle$ are generated in several domains within the linewidth.

Angular spectra. Similarly, if one selects the frequencies of the two photons, for instance, corresponding to exact degeneracy, then the state can be written as the angular spectrum,

$$|\Psi\rangle = \int_0^\infty d\theta \text{sinc}\left(\frac{B\theta}{2}\right) [a_H^\dagger(\theta)a_V^\dagger(-\theta)e^{i\frac{B\theta}{2}} + a_V^\dagger(\theta)a_H^\dagger(-\theta)e^{-i\frac{B\theta}{2}}] |\text{vac}\rangle, \quad (6)$$

Hence, the same 'fine structure' of Bell states is present within the angular lineshape of SPDC. Similarly to the frequency case, this structure can be removed or made finer by, respectively, reducing (compensating) or increasing the anisotropy. Compensation of the anisotropy can be achieved if an anisotropic plate is placed after the crystal; for example, a similar crystal with the length twice smaller and the optic axis rotated 180° with respect to the pump axis. However, in this case one should avoid SPDC generation in the second crystal. This can be easily achieved by either eliminating the pump after the first crystal or slightly detuning the orientation of the optic axis of the second crystal from exact phase matching. In the last case the resulting change in the B value can be compensated for by choosing a crystal of length slightly differing from $L/2$.

It is worth mentioning that the fine structure is absent if the angle is scanned in the plane orthogonal to the plane of the optic axis.

II.2 Type I phase matching

Consider now generation of polarization-entangled photon pairs by placing two type-I crystals one after the other into a common pump beam, the optic axes of the crystals being in orthogonal planes. In the following we consider the case where the pump gives equal contributions to the SPDC intensities in both crystals (i.e. its polarization is at 45° w.r.t. the optic axis planes of the crystals). For this configuration, there are two substantial differences from the type-II case considered above. First, the wavevector mismatch should be expanded up to quadratic terms in the angle and frequency offsets, since the linear terms cancel each other:

$$\Delta_z(\theta, \Omega) \simeq \frac{d^2k_o}{d\Omega^2}\Omega^2 - k_o\theta^2. \quad (7)$$

The form of the mismatch is the same for both crystals. Second, an ordinarily polarized pair born in the first crystal acquires a frequency- and angle-dependent phase factor in the second crystal, where it is extraordinarily polarized, and the state generated at the output is

$$|\Psi\rangle = \iint_0^\infty d\theta d\Omega \text{sinc}\left(\frac{\Delta_z L}{2}\right) \times [a_H^\dagger(\theta, \omega_0 + \Omega)a_H^\dagger(-\theta, \omega_0 - \Omega) + e^{i\phi(\theta, \Omega)}a_V^\dagger(\theta, \omega_0 + \Omega)a_V^\dagger(-\theta, \omega_0 - \Omega)] |\text{vac}\rangle, \quad (8)$$

where, up to second-order terms in frequency and angular offsets, $\phi(\theta, \Omega) = \left(\frac{d^2 k_e}{d\Omega^2} \Omega^2 - k_e \theta^2 + \frac{d^2 k_e}{d\theta^2} \theta^2\right)L$, and the same assumptions on the pump are made as when deriving Eq.(2). The third term in the expression for $\phi(\theta, \Omega)$ is much smaller than the other two and hence can be omitted. As a result, up to the exchange $k_o \rightarrow k_e$, the phase $\phi(\theta, \Omega)$ is equal to the 'mismatch phase' $\Delta_z L$, and the same effect of 'switching' between different maximally entangled states as for the type-II case takes place for this configuration. However, while for the type-II phase matching 'switching' occurred between the states $|\Psi^+\rangle$ and $|\Psi^-\rangle$, this time the Bell states involved are $|\Phi^+\rangle$ and $|\Phi^-\rangle$. The structure of the frequency-angular spectrum in this case is shown in Fig.1b, with the state $|\Phi^+\rangle$ shown by solid lines and the state $|\Phi^-\rangle$ by dashed lines. It is important to emphasize that, a fact that, to our knowledge has not been mentioned yet, also the 'two-type I' scheme of Bell-states preparation requires some filtering: the Bell state produced on the slopes of the spectrum is different from the state produced in the middle.

From Fig.1b one can also observe that, when polarization-entangled states are produced using 'two type-I' phase matching, transition between various maximally entangled states occurs at angles and frequencies where the phase mismatch changes rapidly. This domain is rather narrow; in the most part of the frequency-angular spectrum, only the state $|\Phi^+\rangle$ is produced.

Unlike type-II phase matching, here the 'fine structure' of the angular lineshape appears regardless of the plane where the angular scanning is made.

Frequency and angular spectra. The frequency spectrum of the state in the collinear case is

$$|\Psi\rangle = \int_0^\infty d\Omega \text{sinc}\left(\frac{d^2 k_o}{d\Omega^2} \frac{\Omega^2 L}{2}\right) \times [a_H^\dagger(\omega_0 + \Omega) a_H^\dagger(\omega_0 - \Omega) + e^{i\frac{d^2 k_e}{d\Omega^2} \Omega^2 L} a_V^\dagger(\omega_0 + \Omega) a_V^\dagger(\omega_0 - \Omega)] |\text{vac}\rangle, \quad (9)$$

and the angular spectrum in the degenerate case is

$$|\Psi\rangle = \int_0^\infty d\theta \text{sinc}\left(\frac{k_o \theta^2 L}{2}\right) \times [a_H^\dagger(\theta) a_H^\dagger(-\theta) + e^{ik_e \theta^2 L} a_V^\dagger(\theta) a_V^\dagger(-\theta)] |\text{vac}\rangle. \quad (10)$$

III. EXPERIMENT: POLARIZATION-FREQUENCY ENTANGLEMENT

The general experimental setup for exploring the frequency-angular Bell states structure inside the bandwidth is sketched in Fig.2. Two-photon light generated in

a 0.5 mm type-II crystal or a combination of 1 mm type-I crystals was split using a non-polarizing beamsplitter and a Glan prism was put into each output port. In one of the output ports, angular or frequency selection was performed, the detector in the other arm collecting all possible conjugate modes. Coincidences of the two detectors were measured depending on the positions of the Glan prisms and the frequency and angle selected.

In particular, in the specific experimental setup for testing polarization-frequency Bell states, produced within the bandwidth of collinear frequency-degenerate SPDC, a diffractive-grating monochromator with the resolution 0.8 nm was used as the frequency-selective element. Since the pump was continuous-wave, frequency selection for one of the photons of a pair automatically selected the frequency of the correlated photon. To reduce the contribution of accidental coincidences, a broadband interference filter centered around 702 nm was placed after the beamsplitter. Biphoton pairs were registered by two photodetection apparatuses, consisting of red-glass filters, pinholes, focusing lenses and avalanche photodiodes. The photocount pulses of the two detectors, after passing through delay lines, were sent to the START and STOP inputs of a time-to-amplitude converter (TAC). The output of the TAC was finally addressed to a multi-channel analyzer (MCA), and the number of photocount coincidences of the two detectors was observed at the MCA output.

In a modified version of this setup, an optical fibre was used as a frequency-selective element. Indeed, as it was shown in [16], due to the group-velocity dispersion, an optical fibre performs a Fourier transformation of the two-photon spectral amplitude, which can be measured through the time distribution of the signal-idler delay after the fibre. Thus, in some of our measurements the monochromator in one output port was replaced by an optical fibre of length 1 km inserted into the beam before the beamsplitter. This specific set-up is interesting for application to long-distance fiber quantum communication as the transmission fibre takes the role of transforming the frequency selection to (very easily implementable) time window selection.

III.1 Type-II configuration.

According to Eq.(5), the frequency spectrum of the type-II configuration contains a continuum of polarization-frequency entangled states from $|\Psi^+\rangle$ to $|\Psi^-\rangle$. A usual test of such states consists of fixing one of the polarization prisms at an angle $\Theta_1 = 45^\circ$ and measuring the coincidence counting rate as a function of the other prism orientation Θ_2 (polarization interference). For Bell states $|\Psi^\pm\rangle$, high interference visibility (100% in the ideal case) should be observed, the coincidence counting rate depending on Θ_1, Θ_2 as $R_c \sim \sin^2(\Theta_2 \pm \Theta_1)$ and

its minimum corresponding to $\Theta_2 = \mp 45^\circ$.

To demonstrate the generation of various polarization-entangled states within the collinear type-II SPDC bandwidth, we measured the coincidence counting rate versus the wavelength selected by the monochromator, for two settings of the Glan prisms: $\Theta_1 = 45^\circ, \Theta_2 = -45^\circ$ and $\Theta_1 = \Theta_2 = 45^\circ$ (Fig.3). The results fit well the dependence, calculated in [16] as

$$R_c(\Omega) = \text{sinc}^2(\Omega\tau_0)[\sin^2(\Theta_1 + \Theta_2) \cos^2(\Omega\tau_0) + \sin^2(\Theta_1 - \Theta_2) \sin^2(\Omega\tau_0)]. \quad (11)$$

As it follows from Eq.(11) and is confirmed by experimental spectra (Fig.3), with some specific choice of the wavelengths high-visibility polarization interference is observed when rotating the polarization prism in channel 2. This is well-known for the case where the selected wavelength is the central one. Indeed, by selecting the wavelength of 702 nm and rotating the Glan prism in channel 2 we observed polarization interference with a visibility of 89%. However, we see that high-visibility polarization interference also takes place when the selected wavelength is 695.5 nm or 708.5 nm. Both cases correspond to the selection of the $|\Psi^-\rangle$ state.

To demonstrate polarization interference for the $|\Psi^-\rangle$ state, the wavelength transmitted by the monochromator was fixed at 708.5 nm and the coincidence counting rate was measured depending on the orientation of polarizer 2, the other polarizer being oriented at $\Theta_1 = 45^\circ$. The dependence, shown in Fig.4, demonstrates a visibility of 98%.

Finally, we have checked the invariance of the produced $|\Psi^-\rangle$ state under polarization transformations, which were performed by placing quarter- and half- wave plates (QWP and HWP) at various orientations in front of the beamsplitter. For each setting of the plates, the spectra similar to the ones shown in Fig.3 were obtained. In particular, the dependencies obtained for various HWP orientations are shown in Fig.5(a,b). As expected from the theoretical prediction, the coincidence counting rate corresponding to the wavelengths 695.5 nm and 708.5 nm (the $|\Psi^-\rangle$ state) at both positions of the Glan prisms, $(45^\circ, 45^\circ)$ and $(45^\circ, -45^\circ)$, does not change depending on the HWP orientation, i.e., depending on the rotation of the two-photon polarization state before the beamsplitter. The resulting visibility of polarization interference exceeds 84% for all settings of the HWP. At all other wavelengths (including the central one, 702 nm), the coincidence counting rate clearly depends on the HWP orientation, and for some orientations, the visibility of polarization interference becomes zero. Similar behavior is observed for a QWP inserted before the beamsplitter.

The invariance of the $|\Psi^-\rangle$ state to polarization transformations is also clearly seen when an optical fibre is used as a spectral-selecting element. Indeed, the polar-

ization drift, unavoidably present in optical fibres, 'deteriorates' all the Bell states except the singlet one $|\Psi^-\rangle$. To demonstrate this, we have removed the monochromator and selected the singlet state by means of a 1 km fibre inserted before the beamsplitter. Coincidence distributions obtained for the $(45^\circ, 45^\circ)$ and $(45^\circ, -45^\circ)$ settings of the Glan prisms are presented in Fig.6. One can see that at time delays not corresponding to the generation of the singlet state, the dependencies have complicated shapes and do not correspond to the behavior shown in Fig.3 (a result of polarization drift in the fibre). At the same time, at points pertaining to the $|\Psi^-\rangle$ generation there is a coincidence minimum for the $(45^\circ, 45^\circ)$ settings and a maximum for the $(45^\circ, -45^\circ)$ settings of the prisms.

Using an optical fibre as a frequency-selecting element in the analysis of the two-photon spectral amplitude is most convenient whenever polarization drift can be eliminated or made inessential. In particular, one can use a Faraday mirror (which acts as a time reversal) and make the two-photon light travel twice through the same fibre, thus compensating for the polarization drift. This technique, suggested in [17], was used for two-photon spectral amplitude selection in [16].

Another way to avoid the influence of polarization drift in the fibre is to insert a single Glan prism before the fibre and no prisms after the fibre. Then the role of both Glan prisms is played by a single one, oriented at 45° ; the payoff for eliminating polarization drift is the impossibility to study the coincidence spectrum in the $(45^\circ, -45^\circ)$ configuration. Using this technique, with a 1 km fibre we demonstrated the action of birefringent plates on the state produced at various wavelength of SPDC bandwidth (Fig.7).

According to the considerations given in Section II, if a birefringent plate introducing an e-o delay τ is inserted after the crystal, the spectral dependencies (11) become

$$R_c(\Omega) = \text{sinc}^2(\Omega\tau_0)[\sin^2(\Theta_1 + \Theta_2) \cos^2(\Omega(\tau_0 + \tau)) + \sin^2(\Theta_1 - \Theta_2) \sin^2(\Omega(\tau_0 + \tau))]. \quad (12)$$

As mentioned above, for a complete compensation of the e-o delay, $\tau = -\tau_0$, the state produced is $|\Psi^+\rangle$ over the whole bandwidth. Here we demonstrate the opposite effect, where τ is of the same sign as τ_0 , and the fine structure of the SPDC line becomes even finer. In particular, when $\tau = \tau_0$, the modulation period in (12) becomes twice as large as in (11), and $|\Psi^+\rangle$ is produced at the same pair of frequency offsets $\Omega = \pm\pi/2\tau_0$ where $|\Psi^-\rangle$ is produced in the absence of the birefringent plate.

Indeed, in Fig.7 one can see that the modulation of the SPDC lineshape observed in coincidences becomes more and more frequent as we pass from no plates inserted (Fig.7a) to one quartz plate of thickness 1 mm (Fig.7b) and two quartz plates of thickness 1 mm (Fig.7c) inserted after the BBO crystal.

III.2 'Two type-I' configuration.

With the same experimental setup (and the frequency selection performed by a monochromator), we have analyzed the frequency structure of polarization-entangled states produced by two 1 mm type-I BBO crystals cut for collinear frequency-degenerate phasematching with the optic axes oriented in orthogonal planes. The polarization of the pump was rotated to 45° by a half-wave plate, thus providing equal contributions from each crystal. The phase between the contributions from both crystals at the central wavelength 702 nm was set to zero by tilting two quartz plates with optic axes oriented vertically, placed into the two-photon beam. As it follows from Eq. (9), in this case the lineshape of SPDC contains a continuous set of polarization-entangled states from $|\Phi^+\rangle$ at the center to $|\Phi^-\rangle$ at the slopes, with $\frac{|HH\rangle + e^{i\theta}|VV\rangle}{\sqrt{2}}$ ($0 < \theta < \pi$) entangled states between them. When the orientations of the prisms Θ_1, Θ_2 are varied, maximum visibility of polarization interference is achieved for the Bell states $|\Phi^\pm\rangle$; the coincidence counting rate depends on Θ_1, Θ_2 as $R_c \sim \cos^2(\Theta_1 \mp \Theta_2)$.

Spectral distributions of coincidences for the $(45^\circ, 45^\circ)$ and $(45^\circ, -45^\circ)$ configurations of the Glan prisms are shown in Fig.8. The theoretical dependence, similarly to (11), can be written as

$$R_c(\Omega) = \text{sinc}^2\left(\frac{d^2k_o \Omega^2 L}{d\Omega^2 2}\right) \times [\cos^2(\Theta_1 - \Theta_2) \cos^2\left(\frac{d^2k_e \Omega^2 L}{d\Omega^2 2}\right) + \cos^2(\Theta_1 + \Theta_2) \sin^2\left(\frac{d^2k_e \Omega^2 L}{d\Omega^2 2}\right)]. \quad (13)$$

We see that the Bell states $|\Phi^+\rangle$ and $|\Phi^-\rangle$ are produced when the wavelengths selected are the central one (702 nm) and the side ones (658 nm or 746 nm), respectively. Polarization interference for these states was observed by selecting the corresponding wavelength, fixing one of the Glan prisms at $\Theta_1 = 45^\circ$, and rotating the other one (Fig.9).

Note that although it is commonly believed that the 'two type I crystals' scheme for polarization-entangled production requires neither delay compensation nor filtering, from Fig. 8 one can see that on the slopes of the spectrum, the state produced is different from the one generated in the middle. Note that this occurs even when perfectly collinear SPDC beam ($\theta = 0$) is selected. Hence, filtering the SPDC linewidth is also necessary in this case, although the bandwidth of the filter can be rather large (from Fig. 8, about 30 nm).

IV. EXPERIMENT: POLARIZATION-WAVEVECTOR ENTANGLEMENT

After analyzing frequency structure of the entanglement in type-II or 'two type-I' configurations of SPDC, let us pass to considering its angular structure. It was studied by means of the experimental setup shown in Fig.10 where angular selection was performed in one output port of the beamsplitter. For this purpose, we used a lens with the focal length 500 mm, and the detector apparatus placed in its focal plane. The detector apparatus included an avalanche photodiode, an interference filter with FWHM=3 nm, centered at the degenerate wavelength 702 nm, a lens with focal length 25 mm, and a pinhole with 1 mm diameter. Thus, the angular resolution in the angle-selective arm of the setup (arm 1) was 2 mrad. It is important that, since the detection apparatus was placed into the far-field zone, transverse walk-off effects did not contribute to the results.

The other arm of the setup (arm 2) was designed to collect all angular width of SPDC spectrum corresponding to the degenerate frequency. For this purpose, we removed the lens from the detection apparatus of arm 2 and imaged the pump beam waist (1.5 mm) onto the sensitive area of the avalanche photodiode ($200\mu \times 200\mu$) with a demagnification of 1 : 6. This was obtained by using an objective lens with a large numerical aperture and with the focal length $F = 100$ mm. The angular bandwidth of SPDC after the lens, although increased 6 times, was still within the acceptance angle of the photodiode. In order to prevent a significant contribution of accidental coincidences, an interference filter with FWHM=1 nm and a vertical slit of diameter 2 mm were placed before the detector.

IV.1 Type-II configuration.

In the case of type-II SPDC from a 0.5 mm BBO crystal, we studied the coincidence counting rate distribution using two geometries of experiment. In the first geometry, the angle was scanned in the plane of the optic axis. The corresponding dependence of the coincidence counting rate on the angle selected by the pinhole in arm 1 of the setup, for the $(45^\circ, 45^\circ)$ and $(45^\circ, -45^\circ)$ settings of the Glan prisms, is shown in Fig.11. The dependencies are well fitted by the relation

$$R_c(\theta) = \text{sinc}^2\left(\frac{B\theta L}{2}\right) [\sin^2(\Theta_1 + \Theta_2) \cos^2\left(\frac{B\theta L}{2}\right) + \sin^2(\Theta_1 - \Theta_2) \sin^2\left(\frac{B\theta L}{2}\right)], \quad (14)$$

which follows from Eq.(6). Similarly to the case of the frequency spectrum, the state generated at the center of

the angular lineshape is $|\Psi^+\rangle$, while at the angles ± 0.012 rad the state $|\Psi^-\rangle$ is produced. Indeed, by selecting the angle in arm 1 to be $\theta = 0$, fixing the Glan prism in arm 1 at 45° and rotating the other Glan prism we obtained a polarization interference typical of $|\Psi^+\rangle$, with a visibility of 96.3%. At the same time, the same measurement performed for the angle $\theta = 0.01$ rad selected, showed a polarization-interference dependence typical of $|\Psi^-\rangle$, with the visibility 97% (Fig.12).

In the other geometry of experiment, the angle of scattering was scanned in the plane orthogonal to the plane of the optic axis. As mentioned in Section II, in this case no 'fine structure' of the angular lineshape should be observed since the wavevector mismatch Δ_z is symmetric with respect to the interchange of the wavevectors k_o, k_e . As a result, the produced state was $|\Psi^+\rangle$ for all angles of scattering θ , and the number of coincidences recorded for $(45^\circ, 45^\circ)$ settings of the polarizers by far exceeded the one obtained for $(45^\circ, -45^\circ)$ settings (Fig.13).

IV.2 'Two type-I' configuration.

With a similar experimental setup (Fig.10) we performed the measurements of the spatial spectra in the configuration with two type I crystals with orthogonal optic axes. It is worth mentioning that in this case it is critical that two production crystals are mounted face to face. This arrangement allows to avoid the spatial walk-off between the correlated beams produced from different crystals which leads to their spatial distinguishability. Notice that the problem of the walk-off is absent for the collinear operation. Similar to the previous section we studied the coincidences dependence on the angle selected by the pinhole at a fixed orientations of the polarizers P1 and P2. The quartz plates installed in the pump beam were aligned in a way that the entangled $|\Phi^+\rangle$ state was generated in the collinear configuration. If the pinhole filters a small angle θ within the line of SPDC then the generated state is given by (10). In this case the dependence of the coincidences counting rate is given by (similar to (14)):

$$R_c(\theta) = \text{sinc}^2\left(\frac{k_o\theta^2 L}{2}\right) \left[\sin^2(\Theta_1 + \Theta_2) \cos^2\left(\frac{k_e\theta^2 L}{2}\right) + \sin^2(\Theta_1 - \Theta_2) \sin^2\left(\frac{k_e\theta^2 L}{2}\right) \right] \quad (15)$$

The results of the experiment for the orientations of the polarizers at $(45^\circ, 45^\circ)$ and $(45^\circ, -45^\circ)$ are presented in Fig.14. As one expects from the theoretical considerations (see section II) whilst an entangled $|\Phi^+\rangle$ state is generated within the wide angular bandwidth near the collinear configuration, at side-bands of the spectra the state is transformed into the orthogonal $|\Phi^-\rangle$ state.

V. CONCLUSION

Finally, let us drive some conclusions from the obtained theoretical and experimental results.

Having analyzed two possible schemes for producing polarization-entangled states via cw-pumped SPDC in a crystal of finite length L (usual type-II phasematching and the 'two type-I' scheme), we see that within the natural bandwidth, there is never a single Bell state produced for all mismatch values. At angles and frequencies corresponding to exact phase matching, the Bell state $|\Psi^+\rangle$ is produced for type-II SPDC and the Bell state $|\Phi^+\rangle$, for the 'two type-I' scheme. However, at the values of the phase mismatch $\pm\pi/L$, the state produced in these two schemes is $|\Psi^-\rangle$ and $|\Phi^-\rangle$, respectively. At intermediate mismatches, other maximally entangled states are produced. Since the mismatch variation can be performed through the variation of either frequency or angle of scattering, or both, there is a 'fine structure' of maximally entangled states generation in the two-dimensional frequency-angular spectrum of SPDC.

It is well-known that for type-II SPDC, one can produce the state $|\Psi^+\rangle$ within the whole frequency bandwidth by compensating the delay between the two orthogonally polarized photons of a pair born in the same crystal. This is usually done by placing after the crystal a birefringent plate of appropriate thickness. However, this compensation, although increasing the efficiency of Bell-states generation, still leaves the fine structure in the angular lineshape. To avoid the generation of other Bell states, in all existing experiments one usually selects a sufficiently small angular width by means of a pinhole. From our consideration, it immediately follows that the fine structure of Bell-states generation within the angular SPDC linewidth can be compensated similarly, by placing an anisotropic crystal into the SPDC beam. This would lead to a much more efficient Bell-states generation compared to the case of selecting a narrow angular spectrum.

The case of non-compensated fine structure of Bell states production within the natural SPDC linewidth is also very interesting. An important point that has been evidenced is that the frequency structure can be made to vary more rapidly if the birefringent plate after the crystal increases the e-o delay, instead of reducing it. The advantage of having such a structure is that one can produce different collinear Bell states at non-degenerate wavelengths. They can find application in realizing, for instance, quantum information protocols involving the singlet state and one of the triplet states, e.g. [18].

The fact that the frequency structure is rather narrow (for a type-II crystal of thickness 0.5 mm, it is on the order of ten nanometers) is not a drawback. Indeed, if the Bell states produced are to be applied for quantum communication, which is usually performed through optical

fibres, large wavelength separation should be avoided because of the polarization-mode dispersion. At the same time, we have shown that selection of the wavelength can be in this case performed by means of the fibre itself, through the time selection of the two-photon amplitude.

The possibility to select a Bell state by means of appropriate angular filtering may be of considerable importance since the angular filtering can be principally lossless. This can be used in applications where losses are crucial such as, for instance, squeezed states generation.

The observed fine structure of SPDC lineshape can be also applied in quantum information for the preparation of complex entangled states, for instance, states with double entanglement in frequency, wavevector, and polarization.

Finally, it is worth mentioning that, although here we only considered collinear frequency-degenerate SPDC, the same effects are also present in the non-collinear or frequency non-degenerate cases.

Acknowledgements: We would like to acknowledge Marco Terzi, Ivo DeGiovanni, Luca Giacone and Valentina Caricato for fruitful discussions and help with the experiment. This work was supported in part by the joint grant RFBR-Piedmont 07-02-91581-ASP, by italian minister of research (PRIN 2005023443-002) and by Regione Piemonte (E14).

Sergienko, Phys. Rev. A 50, 5122 (1994).

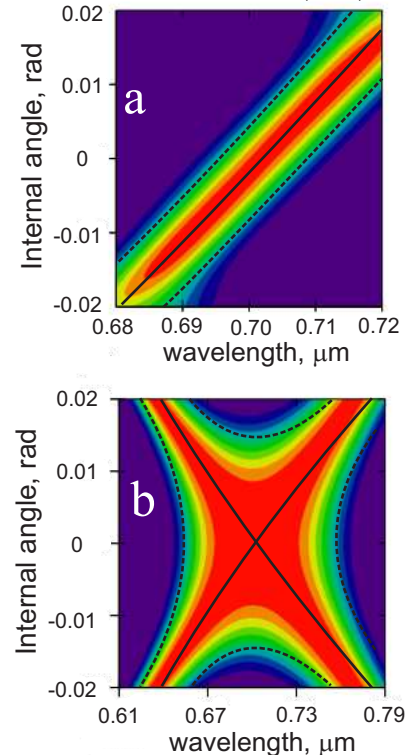


FIG. 1: Frequency-angular distributions of SPDC calculated for the case of (a) type-II collinear frequency-degenerate phase matching in a 0.5 mm BBO crystal and (b) two 1 mm type-I BBO crystals cut for collinear frequency-degenerate phase matching, placed one after another, with optic axes in orthogonal planes, and pumped by the same laser beam (supposed to have a wavelength of 351 nm). Solid lines in (a) show the domains where $|\Psi^+\rangle$ is generated, dashed lines, where $|\Psi^-\rangle$ is generated. Solid lines in (b) show the domains where $|\Phi^+\rangle$ is generated, dashed lines, where $|\Phi^-\rangle$ is generated.

-
- [1] M.A. Nielsen and I.L. Chuang, "Quantum Computation and Quantum Information", Cambridge Univ. press (Cambridge, 2000). D. Bouwmeester et al., "The physics of Quantum Information", Springer Verlag (Berlin, 2000).
- [2] M.Genovese, *Phys. Rep.* **413** 319 (2005).
- [3] G. Brida, M.Genovese, M. Gramegna, *Laser Physics Letters* **3** (2006) 115 and Refs. therein.
- [4] L.A. Lugiato, A. Gatti and E. Brambilla, *J. Opt. B. Quant. Sem. Opt.* **4** (2002) S176.
- [5] A. Garuccio, in "Fundamental Problems in Quantum Theory", Ed. D. Greenberger, (New York Academy of Sciences, 1995).
- [6] P.G.Kwiat, K.Mattle, H.Weinfurter, A.Zeilinger, A.V.Sergienko, Y.H.Shih. *Phys. Rev. Lett.* **75**, 4337 (1995).
- [7] D.Branning, W. P. Grice, R. Erdmann, and I. A. Walsley, *Phys. Rev. Lett.* **83**, 955 (1999);
- [8] Y.-H. Kim, S. P. Kulik, M. V. Chekhova, W. P. Grice, and Y. H. Shih, *Phys. Rev. A* **67**, 010301(R) (2003).
- [9] P.G.Kwiat, E.Waks, A.G.White, I.Appelbaum, and P.G.Eberhard, *Phys. Rev. A* **60**,R773 (1999); G. Brida et al., *Phys. Lett. A* **268**, 12 (2000); **A299**, 121 (2002).
- [10] Y.H.Kim, S.P.Kulik, and Y.H.Shih. *Phys. Rev. A* **63**, 060301(R) (2001).
- [11] A.V.Burlakov, S.P.Kulik, G.O.Rytikov, and M.V.Chekhova, *JETP* **95**, 639-644 (2002).
- [12] M. H. Rubin, D. N. Klyshko, Y. H. Shih, and A. V. Sergienko, *Phys. Rev. A* **50**, 5122 (1994).
- [13] L.J.Wang, C.K.Hong, and S.R.Friberg, *J. Opt. B: Quantum and Semiclass. Opt.* **3**, 346 (2001); J. E. Sharping, M. Fiorentino, and P. Kumar, *Opt. Lett.* **26**, 367369 (2001); H.Takesue and K.Inoue, *Phys. Rev. A* **70**, 031802(R) (2004); J.G.Rarity *et al.*, *Optics Express*, **13**, No 2, 534 (2005).
- [14] D.N.Klyshko, *Photons and Nonlinear Optics* (Gordon and Breach, New York, 1988).
- [15] A. V. Burlakov, M. V. Chekhova, D. N. Klyshko, S. P. Kulik, A. N. Penin, Y. H. Shih, and D. V. Strekalov, *Phys. Rev. A* **56**, 32143225 (1997).
- [16] G. Brida, M. V. Chekhova, M. Genovese, and L. A. Krivitsky, *Phys. Rev. Lett.* **96**, 143601 (2006); *Phys. Rev. A* **75**, 015801 (2007); *Journ. of Phys. A*, in press.
- [17] Martinelli M. 1992 *Journ. Mod. Opt.* **39** 451; Martinelli M. 1989 *Opt. Comm.* **72** 341; Breguet J. and Gisin N. 1995 *Opt. Lett.* **20**1447.
- [18] K.Banaszek, A.Dragan, W.Wasilewski, and Czeslaw Radzewicz. *Phys. Rev. Lett.* **92**, 257901 (2004).

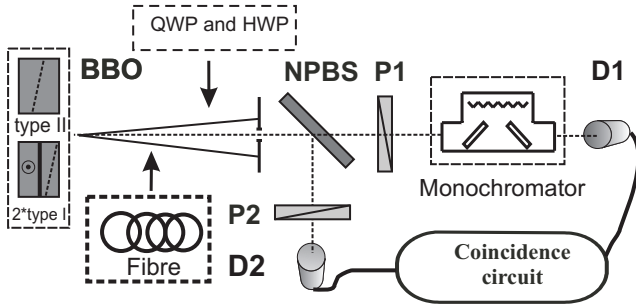


FIG. 2: Scheme of the experimental setup. A type-II BBO crystal or a combination of two type-I crystals cut for collinear frequency-degenerate phase-matching is pumped by cw Ar^+ laser at 351 nm; NPBS, a 50/50 nonpolarizing BS; P1 and P2, Glan prisms; D1, D2, single-photon counting modules. A frequency-selecting element is placed in one arm; in the other arm, all frequencies are collected. Retardation plates, QWP and HWP, are used to study the invariance of the Bell state $|\Psi^-\rangle$ under polarization transformations. In some measurements, the monochromator is replaced by a 1 km single-mode fiber inserted after the crystal and frequency selection is replaced by time selection.

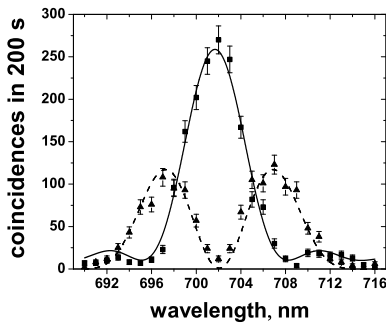


FIG. 3: Experimental dependence of the coincidence counting rate for type-II SPDC on the wavelength selected by the monochromator for two cases: $\Theta_1 = \Theta_2 = 45^\circ$ (squares, solid line) and $\Theta_1 = 45^\circ, \Theta_2 = -45^\circ$ (triangles, dashed line). Lines represent a fit with Eq.(11).

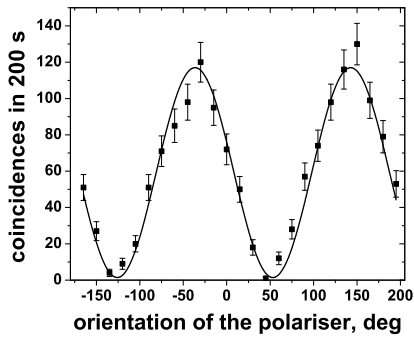


FIG. 4: Polarization interference fringes for the singlet Bell state $|\Psi^-\rangle$ generated in type-II SPDC (the selected wavelength is $\lambda = 708.5\text{nm}$).

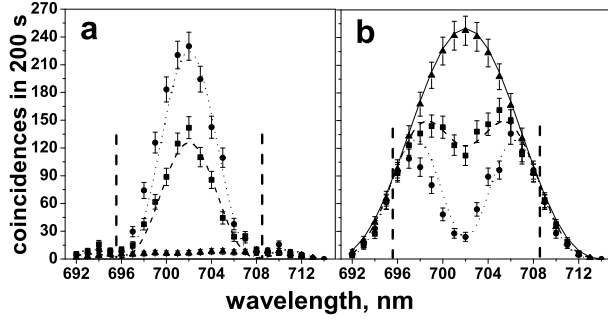


FIG. 5: Experimental dependence of the coincidence counting rate on the wavelength selected by the monochromator for the following orientations of the HWP placed after the crystal: 7° (circles, dotted line); 17° (squares, dashed line); 22.5° (triangles, solid line). Orientations of the Glan prisms are $45^\circ, 45^\circ$ (a) and $45^\circ, -45^\circ$ (b). Dashed vertical bars show the wavelength where $|\Psi^-\rangle$ is generated. Lines represent the theoretical fit.

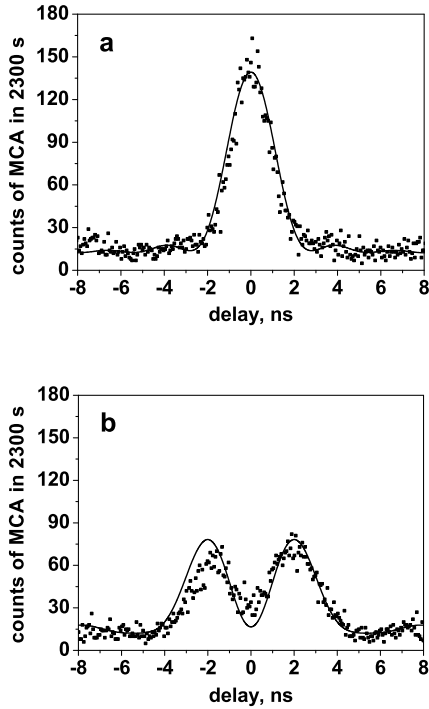


FIG. 6: Experimental dependence of the coincidence counting rate on the delay between the arrivals of two photons, with the monochromator replaced by a 1 km optical fibre and the Glan prisms set at positions (a) $(45^\circ, 45^\circ)$ and (b) $(45^\circ, -45^\circ)$.

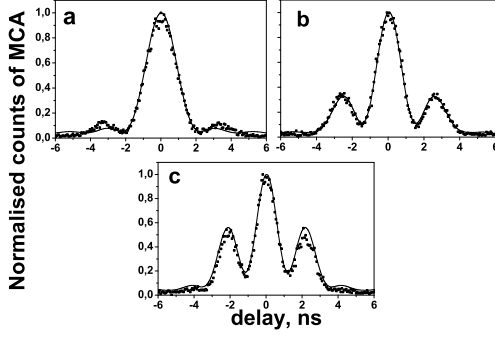


FIG. 7: The measured shape of the second-order correlation function for the case of (a) no quartz plates, (b) one quartz plate of thickness 1 mm, and (c) two quartz plates of thickness 1 mm placed at the output of the crystal with the optic axes parallel to the plane of the BBO optic axis, and a single polarizer set at $\Theta = 45^\circ$ before the fibre. The curves show the theoretical dependencies (12) with an account for the detector jitter time.

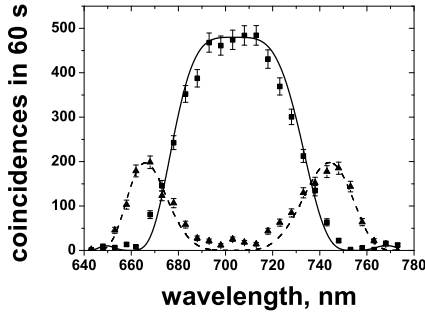


FIG. 8: Experimental dependence of the coincidence counting rate for the 'two-type I' configuration on the wavelength selected by the monochromator for two cases: $\Theta_1 = \Theta_2 = 45^\circ$ (squares, solid line) and $\Theta_1 = 45^\circ, \Theta_2 = -45^\circ$ (triangles, dashed line). Lines represent a fit with Eq.(13).

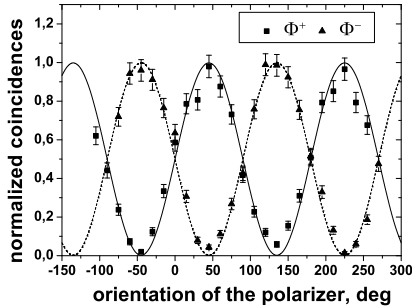


FIG. 9: Polarization interference fringes for the Bell states $|\Phi^+\rangle$ (the selected wavelength is $\lambda = 702\text{nm}$) and $|\Phi^-\rangle$ (the selected wavelength is $\lambda = 658\text{nm}$) generated from the 'two type-I' configuration.

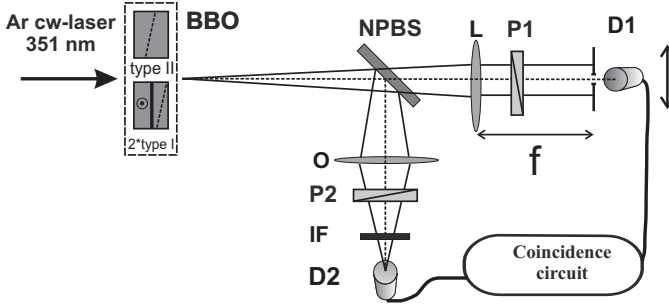


FIG. 10: Scheme of the experimental setup. The crystals arrangement is the same as in fig.2 ; NPBS, a 50/50 nonpolarizing BS; P1 and P2, Glan prisms; D1, D2, single-photon counting modules. Angular selection is performed in one arm by a lens L with focal length 500 mm and a pinhole with diameter 1 mm, placed in a focal plane of L and scanned in the vertical plane together with the detector D1. In the other arm, all angles are collected by means of an objective O with focal length 100 mm. Narrow-band interference filter IF is used to avoid contribution of accidental coincidences.

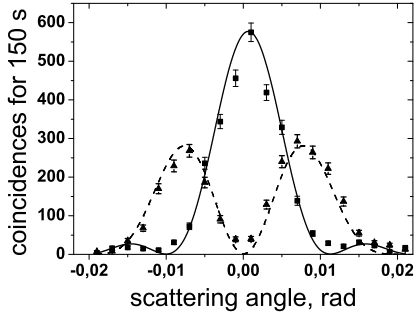


FIG. 11: Experimental dependence of the coincidence counting rate for the 'type II' configuration on the angle selected by the pinhole in arm 1 of the setup for two cases: $\Theta_1 = \Theta_2 = 45^\circ$ (squares, solid line) and $\Theta_1 = 45^\circ, \Theta_2 = -45^\circ$ (triangles, dashed line). Angular scanning was performed in the plane of the optic axis. Lines represent a fit with Eq.(15).

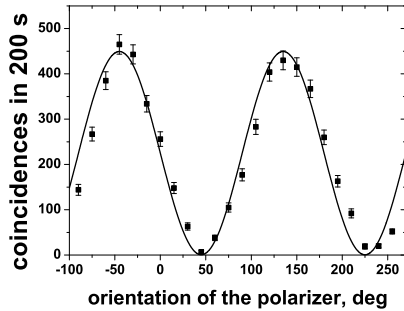


FIG. 12: Polarization interference fringes for the singlet Bell state $|\Psi^-\rangle$ generated in type-II SPDC (the selected angle is $\theta = -0.012$ rad).

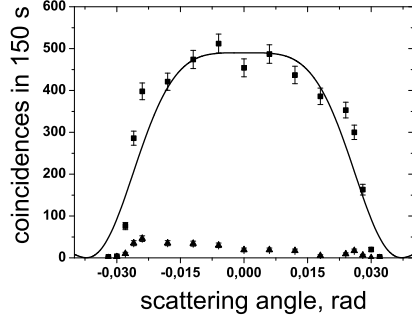


FIG. 13: Experimental dependence of the coincidence counting rate for the 'type II' configuration on the angle selected by the pinhole in arm 1 of the setup for two cases: $\Theta_1 = \Theta_2 = 45^\circ$ (squares, solid line) and $\Theta_1 = 45^\circ, \Theta_2 = -45^\circ$ (triangles, dashed line). Angular scanning was performed in the plane orthogonal to the plane of the optic axis.

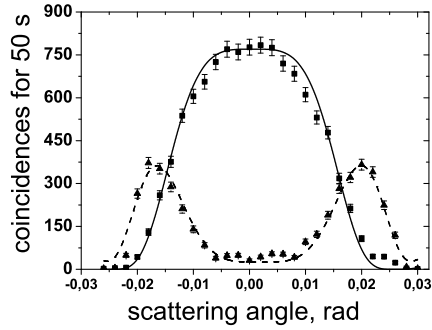


FIG. 14: Experimental dependence of the coincidence counting rate for the 'two-type I' configuration on the angle selected by the pinhole for two cases: $\Theta_1 = \Theta_2 = 45^\circ$ (squares, solid line) and $\Theta_1 = 45^\circ, \Theta_2 = -45^\circ$ (triangles, dashed line).